

Modeling and Analysis of MmWave Communications in Cache-enabled HetNets

Wenqiang Yi, Yuanwei Liu and Arumugam Nallanathan
Queen Mary University of London, London, UK

Abstract—In this paper, we consider a novel cache-enabled heterogeneous network (HetNet), where macro base stations (BSs) with traditional sub-6 GHz are overlaid by dense millimeter wave (mmWave) pico BSs. These two-tier BSs, which are modeled as two independent homogeneous Poisson Point Processes, cache multimedia contents following the popularity rank. High-capacity backhauls are utilized between macro BSs and the core server. A maximum received power strategy is introduced for deducing novel algorithms of the success probability and area spectral efficiency (ASE). Moreover, Monte Carlo simulations are presented to verify the analytical conclusions and numerical results demonstrate that: 1) the proposed HetNet is an interference-limited system and it outperforms the traditional HetNets; 2) there exists an optimal pre-decided rate threshold that contributes to the maximum ASE; and 3) 73 GHz is the best mmWave carrier frequency regarding ASE due to the large antenna scale.

I. INTRODUCTION

To support the explosive data traffic of future fifth-generation (5G) cellular networks, numerous researches [1–4] have paid attention to an innovative framework that densifies the traditional networks with massive small base stations (BSs) or exploiting power domain. However, the improvement of these heterogeneous networks (HetNets) is mainly restricted to the capacity of the backhauls [1]. A recent study [5] has relaxed the limitation by equipping caches at all BSs to store the most popular files as only the minority of multimedia contents is frequently requested by the majority of customers in the real world. Accordingly, the aforementioned cache-enabled HetNets have been studied in various papers. The primary work [6] analyzed the energy efficiency and throughput of cache-enabled cellular networks with a regular hexagonal grid. Since stochastic geometry is a useful tool to acquire the networks' randomness, modeling a tier of BSs in small cell networks or HetNets with a Poisson Point Process (PPP) is more accurate than the traditional hexagonal scenario [7]. Under this condition, the throughput of multi-tier cache-enabled HetNets was discussed in [1], where macro BSs connected to the core networks via backhauls and small cell devices cached the content through wireless broadcasting. Unfortunately, the further analysis on the impact of backhaul capacity was omitted, which is the key parameter when comparing with the conventional HetNets.

In addition to the network densification, another key capacity-increasing technology is exploiting new spectrum bands, such as millimeter wave (mmWave) [8]. Two distinctive characteristics of mmWave are small wavelength and the sensitivity to blockages [9, 10]. Thanks to short wavelength, steerable antennas can be deployed at devices to enhance the

directional array gain [9]. On the other side, the sensitivity gives rise to severe penetration loss for mmWave signals when passing through building exteriors [10], so it is unrealistic to expect the outdoor-to-indoor coverage from macro mmWave BSs. An ingenious hybrid network is created to solve this issue, where mmWave transmitters contribute to the ultra-fast data rate in short-range small cells, and sub-6 GHz BSs provide the universal coverage [11]. The same with cache-enabled HetNets, stochastic geometry has also been wildly utilized in mmWave networks, where the locations of transceivers were modeled following PPPs [12]. With the aid of such structure, the primary article [12] introduced a stochastic blockage model to represent the actual mmWave communication environment, but the antenna pattern was over-simplified as a flat-top model. Then the authors in [13] proposed an actual antenna pattern for increasing the accuracy. Considering the hybrid HetNets, a tractable structure combining mmWave with sub-6 GHz was analyzed in [11], which performed close to the reality.

As discussed above, although HetNets with caches have been fully analyzed under traditional sub-6 GHz networks, there is still lack of articles on a hybrid system with mmWave small cells. Since mmWave is able to provide fast data rate in short-distance networks [14], adopting mmWave into a dense pico tier of cache-enabled HetNets is an promising way to increase the throughput of 5G cellular networks. The other benefit of such hybrid HetNets is no mutual interferences due to applying distinctive carrier frequencies between tiers. These advantages motivate us to create this paper. In contrast to [1], we introduce fiber-connections between macro BSs and the multimedia server to evaluate the impact of backhaul capacity. Then, due to the employment of mmWave, the propagation environment and antenna beamforming pattern in the small cells are replaced by Nakagami fading and actual antenna arrays, respectively. Moreover, we have compared the performance of various mmWave frequencies in this paper. On the other hand, unlike noise-limited assumption in [11], we demonstrate that in the dense mmWave networks, the system becomes an interference-limited scenario. With the aid of the content placement, we conclude that the throughput of our system is conditionally decided by the storage capacity. The main contributions are summarized as follows: 1) we discuss the Laplace transform of interference for traditional sub-6 GHz macro cells and mmWave small cells with the actual antenna pattern; 2) the novel algorithms for the success probability and area spectral efficiency (ASE) under *Maximum Received Power* (Max-RP) scheme are derived; 3)

our model is an interference-limited system and there is an optimum value of rate requirement for obtaining the maximum ASE; and 4) 73 GHz is the best mmWave carrier frequency under the considered association strategy.

II. SYSTEM MODEL

A. Network Architecture

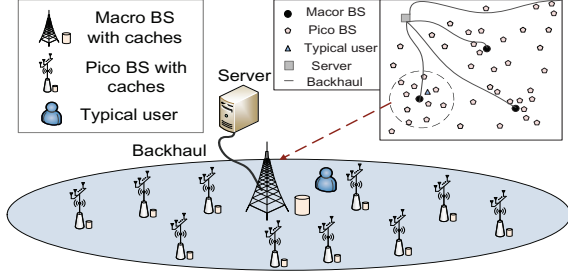


Fig. 1. Layouts of the proposed cache-enabled two-tier hybrid HetNets with traditional macro cells and mmWave small cells.

In this paper, we present a two-tier cache-enabled hybrid HetNet consisting of numerous macro and pico BSs as shown in Fig. 1. The locations of BSs in i -th tier are modeled following an independent homogeneous PPP Φ_i with a density λ_i , where $i = 1$ and 2 represent the macro and pico tier, respectively. In our model, a *typical user* is located at the origin of a plane so that the distribution of distance from the typical user to its nearest BS in i -th tier will follow $p_i(r) = 2\pi\lambda_i r \exp(-\pi\lambda_i r^2)$. Apparently, the number of pico BSs in the real HetNets is much more than that of macro BSs, so we consider $\lambda_1 \ll \lambda_2$. In order to compare the performance of our proposed networks with the traditional HetNets, we provide a server to supply the less-popular contents. This server connects to each macro BS through a high-capacity wired backhaul.

Moreover, different carrier frequencies are employed in our system. The macro BSs connect to receivers with traditional sub-6 GHz, while mmWave is utilized between the pico BS and its corresponding user. As a result, there is no interference between these two tiers. However, in the same tier, other active BSs apart from the *corresponding BS* that serves the typical user will be the source of interferences. Additionally, the quantity of users is assumed to be large enough to ensure that all BSs are active when the corresponding BS is transmitting messages to the typical user.

B. Blockage Model

In tier 1, since macro BSs employ sub-6 GHz as its carrier frequency, the path loss law $L_1(\dot{r})$ with a distance \dot{r} is same with that in traditional cellular networks as shown below

$$L_1(\dot{r}) = C_1 \dot{r}^{-\alpha_1}, \quad (1)$$

where α_1 is the path loss exponent and C_1 is the intercept for the macro tier.

In tier 2, the communication environment is changed due to the employment of mmWave. More specifically, the transmitting routes of pico BSs are divided into line-of-sight (LOS) group and non-line-of-sight (NLOS) group and each of them

has its unique path loss law. Note that the density of the pico tier λ_2 is huge, which indicates that tier 2 can be visualized as dense mmWave networks. One blockage may obstruct all BSs behind it under this case. Therefore, we consider an LOS ball to model the blockage process. A recent study [15] has advocated that such blockage pattern fits the real-world scenarios better than other models. In terms of the NLOS links, the authors in [12] have demonstrated that the impact of NLOS signals is so weak that it can be ignored in mmWave networks, only LOS signals will be considered in this paper.

As a consequence, we define the LOS ball with a radius R_L , which represents the departure from nearby obstacles. The probability of LOS links will be one inside the ball and zero outside the area. The path loss law in tier 2 $L_2(\dot{r})$ with a distance \dot{r} is shown as follows

$$L_2(\dot{r}) = \mathbf{U}(R_L - \dot{r}) C_2 \dot{r}^{-\alpha_2}, \quad (2)$$

where α_2 and C_2 are the path loss exponent and the intercept of LOS links in tier 2, respectively. $\mathbf{U}(x)$ is the unit step function.

C. Directional Beamforming

In i -th tier, we employ antenna arrays composed of N_i elements at all cache-enabled BSs and the transmit power is assumed to be a constant with P_i . The uniform linear array formed by N_2 antenna elements is utilized at all pico BSs. However, we only consider an omnidirectional antenna pattern at macro BSs ($N_1 = 1$) and the typical user for tractability of the analysis [11].

Directional antenna arrays deployed at the pico BSs will supply substantial beamforming gains to compensate the path loss, so the received signal for i -th tier at the typical user can be expressed as follows

$$y_i = \sqrt{C_i}(|x_0|)^{-\frac{\alpha_i}{2}} \mathbf{h}_i^{x_0} \mathbf{w}_i^{x_0} \sqrt{P_i} s_{x_0} + \sum_{x \in \Phi_i \setminus x_0} \sqrt{C_i}(|x|)^{-\frac{\alpha_i}{2}} \mathbf{h}_i^x \mathbf{w}_i^x \sqrt{P_i} s_x + n_0, \quad (3)$$

where interfering BSs are located at x when the typical user is receiving the message from the serving BS at x_0 . The channel vector from the BS to the typical user and the beamforming vector of the BS in i -th tier are denoted by \mathbf{h}_i^x and \mathbf{w}_i^x , respectively. n_0 represents the thermal noise with power σ_i^2 .

Combining with the aforementioned assumptions, the product of the fading gain and beamforming gain of the BS located at x in i -th tier is shown as below [16]

$$H_i^x \triangleq |\mathbf{h}_i^x \mathbf{w}_i^x|^2 = N_i |h_i|^2 G_i(\varphi_x - \theta_x), \quad (4)$$

where h_i is the small fading term for i -th tier. φ_x is the spatial angle of departure (AoD) from the interfering BS to the typical user, and θ_x is the spatial AoD between the BS at location x and its corresponding receiver. $G_i(\cdot)$ is the array gain function. More specifically, an actual array pattern is employed at pico BSs so that $G_2(\omega) \triangleq \frac{\sin^2(\pi N_2 \omega)}{N_2^2 \sin^2(\pi \omega)}$, where ω is a uniformly distributed random variable over $[-\frac{d}{\lambda}, \frac{d}{\lambda}]$. d and λ are the antenna spacing and wavelength, respectively [16]. On the other hand, the array gain function for macro BSs is $G_1(\omega) \triangleq 1$ due to the omnidirectional antenna pattern.

D. Channel Model

Assuming that all active BSs have the full knowledge of the AoD from itself to the typical user, the serving BS will align the antenna beam towards the typical user for achieving maximum directivity gain $G_0 = 1$. In our model, since the corresponding BS is only interfered by the active BSs located in the same tier, the interference for i -th tier can be expressed as follows

$$I_i = \sum_{x \in \Phi_i \setminus x_0} L_i(|x|) H_i^x P_i. \quad (5)$$

Therefore, the signal-to-interference-plus-noise-ratio (SINR) of i -th tier Υ_i at the typical user is given by

$$\Upsilon_i = \frac{L_i(|x_0|) G_0 N_i |h_i|^2 P_i}{\sigma_i^2 + I_i}, \quad (6)$$

where h_2 follows independent Nakagami fading due to utilizing mmWave and the parameter N_2^p of Nakagami fading is considered to be a positive integer for simplifying the analysis [12]. Therefore, $|h_2|^2$ is a normalized Gamma random variable. On the other side, we assume a Rayleigh fading model for the macro tier so that the fading parameter $N_1^p \triangleq 1$.

E. Cache-enabled Content Access Protocol

In this paper, we assume that a static multimedia content catalog containing N_c files is stored at the server. Every macro BSs has a restricted storage with M_1 files, and each of pico BSs has a weaker ability to cache M_2 files, namely, $M_2 < M_1 < N_c$. High-speed backhauls are employed for connecting the core server to macro BSs like traditional HetNets, and the backhaul capacity is denoted by C_{bh} . When the data traffic load of our proposed networks becomes low, the content will be cached in a sequence of its popularity rank at all BSs via broadcasting until the storage is fully occupied. The content with f -th popularity rank can be represented by the Zipf distribution as shown below

$$P_f = \frac{f^{-\delta}}{\sum_{n=1}^{N_c} n^{-\delta}}, \quad (7)$$

where $\delta \geq 0$ is the skew parameter of the probability distribution.

With the aid of Max-RP scheme, the access protocol in our paper is defined as follows.

Access Protocol: When the typical user demands a multimedia file, it communicates with the proximate macro or pico BS with maximum received power. However, if the demanded content is absent from the corresponding BS due to limited storage capacity, the typical user will request that file from the server via the nearest macro BS.

III. LAPLACE TRANSFORM OF INTERFERENCE

The expected value of interference can be derived by *Laplace Transform of Interference*, using which the success probability and ASE for the considered HetNets will be deduced.

A. Laplace Transform of Interference Analysis in Tier 1

In the macro tier, we utilize sub-6 GHz as the carrier frequency, and the fading channel is assumed to be Rayleigh fading. Therefore, the exact expression for Laplace transform of interference can be expressed as below.

Lemma 1: The Laplace transform of interference in the macro tier is given by

$$\mathcal{L}_1(s) = \exp \left(-\pi \lambda_1 r^2 \left({}_2F_1 \left(-\frac{2}{\alpha_1}, 1; 1 - \frac{2}{\alpha_1}; -\frac{s}{r^{\alpha_1}} \right) - 1 \right) \right), \quad (8)$$

where ${}_2F_1(\cdot)$ is the Gauss hypergeometric function.

Proof: The proof procedure is similar as Appendix B in [1], but fading parameter equals to 1 in our case due to Rayleigh fading assumption. ■

B. Laplace Transform of Interference Analysis in Tier 2

Since the path loss exponent of LOS links α_2 is no less than 2 for the practical mmWave networks, we will divide the analysis into two conditions ($\alpha_2 > 2$ and $\alpha_2 = 2$) in order to achieve several closed-form equations.

Lemma 2: Under the condition $\alpha_2 > 2$, the n -th Laplace transform of interference in the pico tier is as follows

$$\mathcal{L}_2^n(s) = \exp \left(-\pi \lambda_2 (R_L^2 - r^2) - \frac{\pi^2 \lambda_2}{2u_1} \sum_{k_1=1}^{u_1} W_n \left(\frac{x_{k_1} d}{\lambda}, s \right) \sqrt{(1 - x_{k_1}^2)} \right), \quad (9)$$

where

$$W_n(\omega, s) = {}_2F_1 \left(-\frac{2}{\alpha_2}, N_2^p; 1 - \frac{2}{\alpha_2}; -\frac{nsG_2(\omega)}{N_2^p r^{\alpha_2}} \right) r^2 - {}_2F_1 \left(-\frac{2}{\alpha_2}, N_2^p; 1 - \frac{2}{\alpha_2}; -\frac{nsG_2(\omega)}{N_2^p R_L^{\alpha_2}} \right) R_L^2, \quad (10)$$

$x_{k_1} = \cos(\frac{2k_1-1}{2u_1}\pi)$, $k_1 = 1, 2, \dots, u_1$, are Gauss-Chebyshev nodes over $[-1, 1]$, and u_1 is a tradeoff parameter between the accuracy and complexity [17, 18]. When $u_1 \rightarrow \infty$, the equality is established.

Numerous actual channel measures [19, 20] have indicated that the path loss exponent of LOS link is 2 under various carrier frequencies, e.g. 28 GHz, 38 GHz and 73 GHz, so we are more interested in the Laplace transform of interference under the condition of $\alpha_2 = 2$. The equation (10) will be changed into

$$W_n(\omega, s) = \frac{nsG_2(\omega)}{N_2^p} \left(F_y \left(\frac{nsG_2(\omega)}{N_2^p R_L^2} \right) - F_y \left(\frac{nsG_2(\omega)}{N_2^p r^2} \right) \right), \quad (11)$$

where

$$F_y(y) = N_2^p \ln \left(1 + \frac{1}{y} \right) - \frac{1}{y(1+y)^{N_2^p-1}} - \sum_{m=1}^{N_2^p-1} \frac{N_2^p}{(1+y)^{N_2^p-m} (N_2^p-m)}. \quad (12)$$

Proof: See Appendix A. ■

IV. SUCCESS PROBABILITY AND AREA SPECTRAL EFFICIENCY ANALYSIS

Before discussing the success probability, we define our *Content Placement* as follows: All BSs in different tiers will choose the most popular contents to store. As a result, the probability $p_{i,f}$ of the condition that i -th tier BSs cache the same copy of f -th ranked file can be expressed as below

$$p_{i,f} = \mathbf{U}(f-1) - \mathbf{U}(f-M_i-1). \quad (13)$$

Therefore, a set of i -th tier BSs containing the f -th ranked file $\Phi_{i,f}$ will form an independent non-homogeneous PPP with the density $p_{i,f}\lambda_i$

From the costumer's perspective, the success probability is an important parameter to appraise the quality of service. In our cache-enabled HetNets, the instantaneous data rate at the typical user exceeding the pre-decided rate threshold R_{th} will contribute to the success probability [1]. As discussed in the previous sections, we conclude that the proposed system has two different processes in sending the multimedia contents: 1) User Association Mode; and 2) Server Mode. We will discuss these two modes in details as below.

A. User Association Mode

The typical user will choose the macro or pico BS with maximum received power as its serving BS. We define the Max-RP association probability when the typical user connects with i -th tier as follows

$$\mathcal{A}_i^P = \mathbb{P}[N_i C_i P_i r^{-\alpha_i} > N_j C_j P_j r^{-\alpha_j}], \quad (14)$$

where $j \neq i$ and $j \in [1, 2]$

Therefore, the probability density function (PDF) of the distance r between the typical user and its serving BS with f -th ranked file in i -th tier is changed into [21]

$$f_{i,f}^P(r) = 2\pi p_{i,f} \lambda_i r \exp(-\pi \sum_{j=1}^2 p_{j,f} \lambda_j \hat{P}_j^{\frac{2}{\alpha_j}} r^{\frac{2}{\alpha_j}}), \quad (15)$$

where $\hat{P}_j = \frac{N_j C_j P_j}{N_i C_i P_i}$ and $\hat{\alpha}_j = \frac{\alpha_j}{\alpha_i}$.

B. Server Mode

In server mode, the nearest Macro BS will act as the relay to retransmit the multimedia file from the server to the typical user. Under this condition, the backhaul capacity will restrict the performance of our system. To simplify the notation, we first derive the coverage probability of tier 1 without considering the cache capacity.

Lemma 3: Since in various articles [1, 11], the noise can be ignored in the traditional cellular networks with sub-6 GHz, we only consider the signal-to-interference-ratio (SIR) instead of SINR for analyzing the performance of tier 1, namely, $\sigma_1^2 = 0$. Under this condition, the coverage probability for no-caching tier 1 is given by

$$P_{Y_1}(\tau) = {}_2F_1\left(-\frac{2}{\alpha_1}, 1; 1 - \frac{2}{\alpha_1}; -\tau\right)^{-1}. \quad (16)$$

Proof: Note that the SIR coverage probability $P_{Y_1}(\tau) = \mathbb{P}[|h_1|^2 > \frac{\tau I_1 r^{\alpha_1}}{N_1 C_1 P_1} | r = \|x_0\|]$ where $|h_1|^2 \sim \exp(1)$ due to

Rayleigh fading assumption. Thus such coverage probability can be expressed as $P_{Y_1}(\tau) = \int_0^\infty \mathcal{L}_1(r^{\alpha_1}) p_1(r) dr$. Note that $\int_0^\infty r \exp(-ar^2) dr = \frac{1}{2a}$, $a > 0$, the coverage probability will be simplified as above. ■

Corollary 1: The success probability $P_S(R_{th})$ in server mode is given by

$$P_S(R_{th}) = \mathbf{U}(C_{bh} - R_{th}) \sum_{f=M_1+1}^{N_c} P_f P_{Y_1}(2^{\frac{R_{th}}{B_1}} - 1). \quad (17)$$

Proof: In server mode, if C_{bh} is smaller than R_{th} , the $P_S(R_{th})$ will be zero as the system rate is not large enough for transmitting the content. Moreover, if C_{bh} is larger than R_{th} , the success probability for f -th ranked file under this mode will be $P_f P_{Y_1}(2^{\frac{R_{th}}{B_1}} - 1)$. We sum up the $(M_1 + 1)$ -th to N_c -th elements to calculate $P_S(R_{th})$ as shown above. ■

C. Success Probability

Based on the Laplace transform of the interference, we are able to calculate the content-related coverage probabilities of two tiers, which is the basement for analyzing the success probability.

Lemma 4: For f -th ranked content, the coverage probability for i -th tier $\Theta_{i,f}(\tau)$ under Max-RP scheme is shown below

$$\Theta_{1,f}(\tau) = \int_0^\infty \mathcal{L}_1(r^{\alpha_1}) f_{1,f}^P(r) dr, \quad (18)$$

$$\begin{aligned} \Theta_{2,f}(\tau) &\approx \frac{\pi R_L}{2u_2} \sum_{n=1}^{N_2^P} (-1)^{n+1} \binom{N_2^P}{n} \\ &\times \sum_{k_2=1}^{u_2} F_R\left(\frac{(x_{k_2}+1)R_L}{2}\right) \sqrt{(1-x_{k_2}^2)}, \end{aligned} \quad (19)$$

where

$$F_R(r) = \mathcal{L}_2^n\left(\frac{\eta_L r^{\alpha_2}}{G_0}\tau\right) \exp\left(-\frac{n\eta_L r^{\alpha_2} \tau \sigma_2^2}{P_2 C_2 N_2 G_0}\right) f_{2,f}^P(r). \quad (20)$$

Proof: Note that the probability of distance under this user association is shown in equation (15), with the similar calculation process with Appendix A from [12] and Lemma 3, coverage probability for two tier can be expressed as above. ■

As mentioned in the beginning of this section, the universal success probability can be defined as below

$$P_s(R_{th}) = \sum_{i=1}^2 \mathcal{A}_i^P \mathbb{P}[B_i \log_2(1 + \Upsilon_i) > R_{th}] + P_S(R_{th}). \quad (21)$$

Theorem 1: With the aid of Corollary 1 and Lemma 4, the success probability of Max-RP will be as follows

$$P_P(R_{th}) \approx \sum_{f=1}^{M_1} \sum_{i=1}^2 P_f \Theta_{i,f}(2^{\frac{R_{th}}{B_i}} - 1) + P_S(R_{th}). \quad (22)$$

Proof: When the required rate is R_{th} , the pre-decided SINR threshold is $(2^{\frac{R_{th}}{B_i}} - 1)$, so the success probability for f -th ranked content in the first M_1 popularity rank is $P_f \Theta_{i,f}(2^{\frac{R_{th}}{B_i}} - 1)$. Considering the whole multimedia contents, the success probability will be calculated as above. ■

D. Area Spectral Efficiency

The ASE is the average instantaneous data rate transmitted in unit bandwidth and unit area. Assuming that Gaussian Codebooks are utilized for all transmissions, we are able to define ASE with the aid of Shannon's Capacity Formula. It is expressed as follows $ASE = \lambda \log_2(1 + \tau) P_\tau$, where P_τ is the SINR coverage probability of the considered networks and λ denotes the active BSs' density [22].

Proposition 1: The ASE \mathbb{A} for Max-RP user association strategy is given by

$$\mathbb{A} = \sum_{f=1}^{M_1} \sum_{i=1}^2 \frac{P_f p_{i,f} \lambda_i R_{th}}{B_i} \Theta_{i,f} (2^{\frac{R_{th}}{B_i}} - 1) + \frac{\lambda_1 R_{th}}{B_1} P_S(R_{th}), \quad (23)$$

V. NUMERICAL RESULTS

The general network settings for our system are shown in Table. I [1, 11, 12] and the reference distance for the intercept is one meter.

TABLE I
GENERAL SETTINGS OF THE NETWORK

LOS ball range	$R_L = 200$ m
Density of tier1	$\lambda_1 = 1/(250^2 \pi) \text{ m}^{-2}$
Density of tier2	$\lambda_2 = 20/(250^2 \pi) \text{ m}^{-2}$
Bandwidth	$B_1 = 20$ MHz; $B_2 = 1$ GHz
Path loss law	$\alpha_1 = 4$; $\alpha_2 = 2$, $N_2^p = 3$
Number of antennas	$N_1 = 1$; $N_2 = 16$
Carrier frequency for two tiers	$f_m = 2$ GHz; $f_p = 28$ GHz
Transmit Power at BSs	$P_1 = 80$ dBm; $P_2 = 30$ dBm
Transmit Power at the typical user	$P_0 = 30$ dBm
Backhaul capacity	$C_{bh} = 500$ Mbps
Number of content	$M_1 = 80$, $M_2 = 10$, $N_c = 100$
Skew of the popularity distribution	$\delta = 0.6$

Fig. 2 illustrates the impact of R_{th} and N_2 on success probability. Comparing the analytical results of the success probability with the simulation results, we note that they match each other ideally, thereby certifying the analysis. It is obvious that our cache-enabled HetNets outperform the traditional HetNets where the macro BSs have no caching capacity, especially in the area $R_{th} \geq C_{bh}$. Moreover, the SIR scenario fits the analytical results perfectly so that our model can be regarded as an interference-limited system. Lastly, with the rise of antenna scales N_2 , the success probability will correspondingly increase.

Fig. 3 shows the success probability versus cache capacity with different P_1 . The success probability has a negative correlation with the transmit power P_1 . Massive P_1 contributes to large received power, when P_1 increases to 100 dBm, the success probability becomes independent on M_1 . In this case, the typical use will associate with tier 1 all the time. In terms of the cache capacity, the success probability is a monotonic increasing function with pico BSs' storage capacity M_2 . For the cache capacity of macro BSs M_1 , when $C_{bh} > R_{th}$, the success probability has no relationship with M_1 since the less-popular content that only contained in the server can be transmitted freely through the backhaul. Under this condition, the proposed HetNet is same with the traditional one. On the other side, when

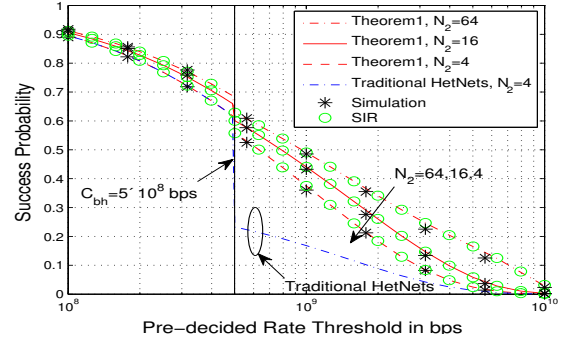


Fig. 2. Success probability versus pre-decided rate threshold with $B_1 = 500$ MHz.

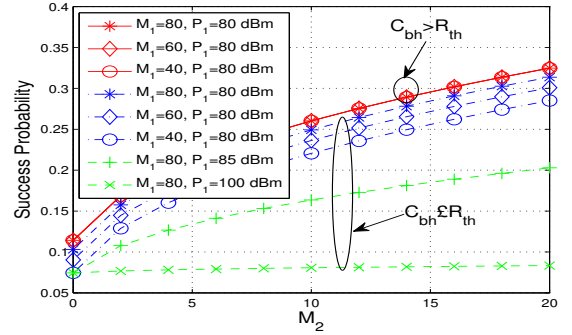


Fig. 3. Success probability versus cache capacity M_2 in tier 2 with different M_1 , P_1 and $R_{th} = 10^8$ bps.

$C_{bh} \leq R_{th}$, the server will be blocked so that the success probability will be benefited by the large M_1 , which represents that more multimedia files can be stored at macro BSs.

Fig 4 plots the ASE versus R_{th} with different λ_2 and carrier frequencies. The optimum pre-decided rate threshold R_{th} for achieving the maximum ASE can be easily figured out due to the convex property. When the density of pico tier λ_2 increases from $10/(250^2 \pi) \text{ m}^{-2}$ to $30/(250^2 \pi) \text{ m}^{-2}$, the optimal number decreases. Then, we compare the carrier frequencies at 28 GHz, 38 GHz, 60 GHz and 73GHz with antenna scales $N_2 = 10, 20$,

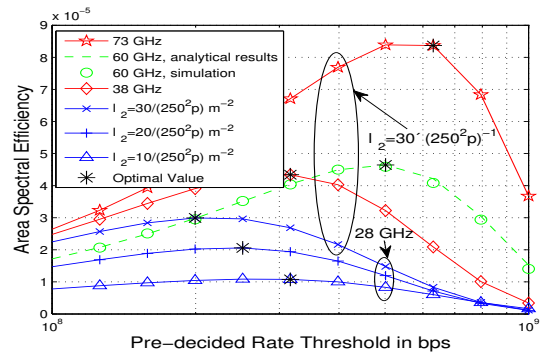


Fig. 4. Area spectral efficiency versus pre-decided rate threshold with different λ_2 , carrier frequencies and $B_1 = 500$ MHz.

40 and 80 [14], respectively. All of them has the same LOS path loss exponents ($\alpha_2 = 2$), except that the path loss exponent for 60 GHz is 2.25 [19, 20]. Fig. 4 illustrates that 73 GHz is the best choice thanks to the largest antenna scales. The simulation of 60 GHz matches the analytical results with an insignificant difference, thereby verifying all analytical expressions under the condition $\alpha_2 > 2$.

VI. CONCLUSION

In this treatise, we utilize the stochastic geometry to analyze the performance of our cache-enabled hybrid HetNet. More specifically, the proposed network, which performs better than the traditional HetNet, can be regarded as an interference-limited system due to the high density of mmWave tier and the nature of sub-6 GHz tier. As discussed in the previous sections, our system has a positive correlation with pico BSs' antenna scales and the cache capacity of both tiers. Additionally, there exists an optimum value of pre-decided rate threshold contributing to the maximum ASE. Lastly, for Max-RP association strategy, 73 GHz is the best carrier frequency of mmWave tier.

APPENDIX A: PROOF OF LEMMA 1

The Laplace transform of interference in tier 2 is given by

$$\begin{aligned}\mathcal{L}_2^n(s) &= \mathbb{E}\left[\exp\left(-ns \sum_{x \in \Phi_2 \setminus x_0} G_2(\omega) |h_2|^2 ||x|^{-\alpha_2}\right)\right] \\ &\stackrel{(a)}{=} e^{-2\pi\lambda_2 \mathbb{E}_{G_2} \left[\int_{r^L}^{R_L} \left(1 - \left(1 + \frac{nsG_2(\omega)}{N_2^p v^{\alpha_2}}\right)^{-N_2^p}\right) v dv \right]} \\ &\stackrel{(b)}{=} e^{-\frac{\pi\lambda_2\lambda}{d} \int_{-\frac{d}{\lambda}}^{\frac{d}{\lambda}} \int_{r^L}^{R_L} \left(1 - \left(1 + \frac{nsG_2(\omega)}{N_2^p v^{\alpha_2}}\right)^{-N_2^p}\right) v dv d\omega},\end{aligned}\quad (\text{A.1})$$

where (a) follows the Gamma random variable's moment generating function [12]; (b) is computing the expectation of tier 2 antenna gain G_2 . When $\alpha_2 > 2$, (A.1) can be simplified as follows

$$\begin{aligned}\mathcal{L}_2^n(s) &\stackrel{(c)}{=} \exp\left(-\pi\lambda_2(R_L^2 - r^2)\right) \\ &\quad - \frac{\pi\lambda_2\lambda}{2d} \int_{-\frac{d}{\lambda}}^{\frac{d}{\lambda}} \left({}_2F_1\left(-\frac{2}{\alpha_2}, N_2^p; 1 - \frac{2}{\alpha_2}; -\frac{nsG_2(\omega)}{N_2^p r^{\alpha_2}}\right) r^2 \right. \\ &\quad \left. - {}_2F_1\left(-\frac{2}{\alpha_2}, N_2^p; 1 - \frac{2}{\alpha_2}; -\frac{nsG_2(\omega)}{N_2^p R_L^{\alpha_2}}\right) R_L^2 \right) d\omega,\end{aligned}\quad (\text{A.2})$$

(c) follows Gauss hypergeometric function. When $\alpha_2 = 2$, (A.1) can be simplified as below

$$\begin{aligned}\mathcal{L}_2^n(s) &\stackrel{(d)}{=} \exp\left(-\pi\lambda_2(R_L^2 - r^2) - \frac{\pi\lambda_2\lambda}{2d} \int_{-\frac{d}{\lambda}}^{\frac{d}{\lambda}} \left(\frac{nsG_2(\omega)}{N_2^p}\right) \right. \\ &\quad \left. \times \left(F_y\left(\frac{nsG_2(\omega)}{N_2^p R_L^2}\right) - F_y\left(\frac{nsG_2(\omega)}{N_2^p r^2}\right)\right) d\omega\right).\end{aligned}\quad (\text{A.3})$$

(d) follows (2.117-1), (2.117-3) and (2.118-1) in [23]. With the aid of Gauss-Chebyshev Quadrature, we obtain **Lemma 1**.

REFERENCES

- [1] D. Liu and C. Yang, "Caching policy toward maximal success probability and area spectral efficiency of cache-enabled HetNets," *IEEE Trans. Commun.*, vol. 65, no. 6, pp. 2699–2714, Jun. 2017.
- [2] J. Zhao, Y. Liu, K. K. Chai, A. Nallanathan, Y. Chen, and Z. Han, "Spectrum allocation and power control for non-orthogonal multiple access in HetNets," *IEEE Trans. Wireless Commun.*, vol. 16, no. 9, pp. 5825–5837, Sep. 2017.
- [3] Y. Liu, Z. Qin, M. ElKashlan, A. Nallanathan, and J. A. McCann, "Non-orthogonal multiple access in large-scale heterogeneous networks," *IEEE J. Sel. Areas Commun.*, vol. 35, no. 12, pp. 2667–2680, Dec. 2017.
- [4] Z. Ding, Y. Liu, J. Choi, Q. Sun, M. ElKashlan, C. L. I, and H. V. Poor, "Application of non-orthogonal multiple access in LTE and 5G networks," *IEEE Commun. Mag.*, vol. 55, no. 2, pp. 185–191, Feb. 2017.
- [5] X. Wang, M. Chen, T. Taleb, A. Ksentini, and V. C. M. Leung, "Cache in the air: Exploiting content caching and delivery techniques for 5G systems," *IEEE Commun. Mag.*, vol. 52, no. 2, pp. 131–139, Feb. 2014.
- [6] D. Liu and C. Yang, "Energy efficiency of downlink networks with caching at base stations," *IEEE J. Sel. Areas Commun.*, vol. 34, no. 4, pp. 907–922, Apr. 2016.
- [7] R. W. Heath, M. Kountouris, and T. Bai, "Modeling heterogeneous network interference using Poisson point processes," *IEEE Trans. Signal Process.*, vol. 61, no. 16, pp. 4114–4126, Aug. 2013.
- [8] Y. Liu, Z. Qin, M. ElKashlan, Z. Ding, A. Nallanathan, and L. Hanzo, "Nonorthogonal multiple access for 5G and beyond," *Proc. IEEE*, vol. 105, no. 12, pp. 2347–2381, Dec. 2017.
- [9] T. S. Rappaport, F. Gutierrez, E. Ben-Dor, J. N. Murdock, Y. Qiao, and J. I. Tamir, "Broadband millimeter-wave propagation measurements and models using adaptive-beam antennas for outdoor urban cellular communications," *IEEE Trans. Antennas Propag.*, vol. 61, no. 4, pp. 1850–1859, Apr. 2013.
- [10] A. V. Alejos, M. G. Sanchez, and I. Cuinas, "Measurement and analysis of propagation mechanisms at 40 GHz: Viability of site shielding forced by obstacles," *IEEE Trans. Veh. Technol.*, vol. 57, no. 6, pp. 3369–3380, Nov. 2008.
- [11] H. Elshaer, M. N. Kulkarni, F. Boccardi, J. G. Andrews, and M. Dohler, "Downlink and uplink cell association with traditional macrocells and millimeter wave small cells," *IEEE Trans. Wireless Commun.*, vol. 15, no. 9, pp. 6244–6258, Sep. 2016.
- [12] T. Bai and R. W. Heath, "Coverage and rate analysis for millimeter-wave cellular networks," *IEEE Trans. Wireless Commun.*, vol. 14, no. 2, pp. 1100–1114, Feb. 2015.
- [13] D. Maamari, N. Devroye, and D. Tuninetti, "Coverage in mmWave cellular networks with base station co-operation," *IEEE Trans. Wireless Commun.*, vol. 15, no. 4, pp. 2981–2994, Apr. 2016.
- [14] W. Yi, Y. Liu, and A. Nallanathan, "Modeling and analysis of D2D millimeter-wave networks with poisson cluster processes," *IEEE Trans. Commun.*, vol. 65, no. 12, pp. 5574–5588, Dec. 2017.
- [15] J. G. Andrews, T. Bai, M. N. Kulkarni, A. Alkhateeb, A. K. Gupta, and R. W. Heath, "Modeling and analyzing millimeter wave cellular systems," *IEEE Trans. Commun.*, vol. 65, no. 1, pp. 403–430, Jan. 2017.
- [16] X. Yu, J. Zhang, M. Haenggi, and K. B. Letaief, "Coverage analysis for millimeter wave networks: The impact of directional antenna arrays," *IEEE J. Sel. Areas Commun.*, vol. 35, no. 7, pp. 1498–1512, Jul. 2017.
- [17] Y. Liu, Z. Qin, M. ElKashlan, Y. Gao, and L. Hanzo, "Enhancing the physical layer security of non-orthogonal multiple access in large-scale networks," *IEEE Trans. Wireless Commun.*, vol. 16, no. 3, pp. 1656–1672, Mar. 2017.
- [18] Y. Liu, Z. Ding, M. ElKashlan, and H. V. Poor, "Cooperative non-orthogonal multiple access with simultaneous wireless information and power transfer," *IEEE J. Sel. Areas Commun.*, vol. 34, no. 4, pp. 938–953, Apr. 2016.
- [19] S. Deng, M. K. Samimi, and T. S. Rappaport, "28 GHz and 73 GHz millimeter-wave indoor propagation measurements and path loss models," in *Prof. IEEE Int. Conf. on Commun. Workshop (ICCW)*, Jun. 2015, pp. 1244–1250.
- [20] T. S. Rappaport, E. Ben-Dor, J. N. Murdock, and Y. Qiao, "38 GHz and 60 GHz angle-dependent propagation for cellular & peer-to-peer wireless communications," in *IEEE Proc. of International Commun. Conf. (ICC)*, Jun. 2012, pp. 4568–4573.
- [21] H. S. Jo, Y. J. Sang, P. Xia, and J. G. Andrews, "Heterogeneous cellular networks with flexible cell association: A comprehensive downlink SINR analysis," *IEEE Trans. Wireless Commun.*, vol. 11, no. 10, pp. 3484–3495, Oct. 2012.
- [22] M. Afshang, H. S. Dhillon, and P. H. J. Chong, "Modeling and performance analysis of clustered device-to-device networks," *IEEE Trans. Wireless Commun.*, vol. 15, no. 7, pp. 4957–4972, Jul. 2016.
- [23] A. Jeffrey and D. Zwillinger, *Table of integrals, series, and products*. Academic press, 2007.